On Spatiotemporal Swath Width of the Lunar-Based SAR Earth Observation under Orbital Perturbations

Zhen Xu[(1)], Kun-Shan Chen*[(2)]

(1) Shantou University, Shantou, China; e-mail: xuzhen@stu.edu.cn;
(2) Guilin University of Technology, Guilin, China; e-mail: chenks@glut.edu.cn.

Abstract

This study analyzes the spatiotemporal swath width in the lunar-based SAR (LBSAR) for Earth observation. The major finding is that the LBSAR's altitude and beamwidth dominate the swath width, and the side-looking direction determines the region covered by LBSAR. Specifically, the left-looking LBSAR is more suitable for monitoring the northern hemisphere of Earth and vice versa. Further, the LBSAR altitude is susceptible to orbital perturbations, leading to aperiodic and irregular temporal variations in the swath width and related coverage. The results also suggest that the LBSAR has great potential for offering a swath width over thousands of kilometers under appropriate configurations.

1 Introduction

The lunar exploration provokes an increasingly revived interest, and plenty of missions have been proposed for building the lunar base [1]. The synthetic aperture radar (SAR) mounted on the lunar base, i.e., the lunar-based SAR (LBSAR), makes it possible to consistently watch Earth with an extensive beam footprint [2]. Under the LBSAR, it is instructive to obtain richer data sets of the globe with a high temporal resolution, which is attractive for monitoring large-scale Earth phenomena. Hence, the LBSAR has aroused growing interest from geoscience and related communities [3].
Built on a natural satellite, the LBSAR exhibits distinctiveness differentiating it from spaceborne SAR. One lies in its ease of being affected by squint effects under the distinctive observation geometry of the LBSAR [4]. In order to acquire high-quality images, it was preferable to apply the zero-Doppler centroid steering to the LBSAR [5]. In this event, the coverage performance, one of the most significant metrics for Earth observation, could be evaluated by the illumination time along the LBSAR path and the swath width that awards the extent of the imaging scene on Earth. Also, the swath width is strongly correlated to the design rationalities of system parameters [6]. Hence, it is of essence to probe into the swath width of the LBSAR, which demands more study.

The LBSAR altitude, in particular, is related to the orbital elements susceptible to perturbation effects [7]. From this perspective, the orbital perturbations could potentially affect the LBSAR swath width, further complicating its spatiotemporal variation. This study quantitatively analyzes the LBSAR swath width under the zero-Doppler steering mode to evaluate its coverage performance. Also, the spatiotemporal variation of swath width in different cycles are examined to show how the orbital perturbations affect the LBSAR swath width and related covered region.

The rest of this paper is organized as follows. Section 2 begins with an observation geometry of LBSAR, followed by illustrations of the swath width and some related bounds. Section 3 discusses the LBSAR configurations based on derived lower and upper bounds and highlights the quantitative analysis of the swath width. Section 4 presents the spatiotemporal swath width under various cycles of the LBSAR, the Earth regions covered by the LBSAR in different periods are also analyzed. Finally, Section 5 summarizes the paper.

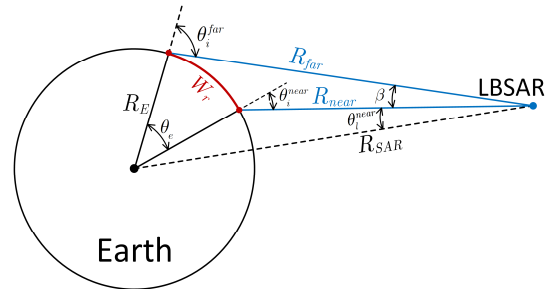## 2 Representations of the Swath Width and Related Bounds in the LBSAR

Figure 1. The observation geometry of the LBSAR.

Figure 1 depicts the swath width in the LBSAR the observation geometry, from which we see that the LBSAR swath width relates to the geocentric angle:

$$\theta_e = \sin^{-1}(R_{SAR}R_E^{-1}\sin\theta_l^{far}) - \sin^{-1}(R_{SAR}R_E^{-1}\sin\theta_l^{near}) - \beta \tag{1}$$

with

$$\theta_l^{far} = \theta_l^{near} + \beta \tag{2}$$

$$R_{SAR} = \left\| \mathbf{R_{SAR(ECI)}} \right\|_2 \tag{3}$$

$$\mathbf{R_{SAR(ECI)}} = \mathbf{R_{EM(ECI)}} + \mathbf{U_{MCI}^{MCMF}}\mathbf{R_{SITE(MCMF)}} \tag{4}$$

where R_E is the Earth's radius, θ_l^{near} and θ_l^{far} are the near and far look angles, β is the beamwidth, $\mathbf{R_{EM(ECI)}}$ is the position of the Moon's barycenter in the Earth Centered Inertial (ECI) coordinate. $\mathbf{R_{SITE(MCMF)}}$ is the LBSAR's site location on the lunar surface, which is given in the Moon Centered Moon Fixed (MCMF) coordinate. $\mathbf{U_{MCI}^{MCMF}}$ is the transformation matrix from the MCMF coordinate to Moon Centered Inertial (MCI) coordinate.

In Eq. (1), the LBSAR beamwidth is given by

$$\beta = \lambda \cdot k_r \cdot l_r^{-1} \qquad (5)$$

where λ is the wavelength, l_r is the aperture length along the range direction, and k_r is the taper factor related to the beam steepness. For a uniformly distributed beam, $k_r = 0.88$, whereas for a highly tapered beam, $k_r \approx 2$ [6].

For the LBSAR, once its site on the Moon's surface is decided, and its configurations are selected, the swath width could be determined by

$$W_r = R_E \cdot \left\{ -\sin^{-1}\left(R_{SAR} R_E^{-1} \sin\theta_l^{near} \right) \right. \\ \left. + \sin^{-1}\left[R_{SAR} R_E^{-1} \sin(\theta_l^{near} + \lambda k_r l_r^{-1}) \right] - \lambda k_r l_r^{-1} \right\} \qquad (6)$$

The target's position within the swath width, signified as $\mathbf{R_{T(ECI)}}$ in the ECI, may be determined by the zero-Doppler centroid steering [5]. For ascertaining the covered region, it is necessary to transform the ECI to the Earth Centered Earth Fixed (ECEF) coordinate in the LBSAR:

$$\mathbf{R_{T(ECEF)}} = \mathbf{U_{ECEF}^{ECI}} \mathbf{R_{T(ECI)}} \qquad (7)$$

where the expressions for matrices $\mathbf{U_{MCI}^{MCMF}}$ and $\mathbf{U_{ECEF}^{ECI}}$ can be found in [6, 8] with additional details.

Certain critical bounds should be clarified in the analysis of LBSAR swath width. First is the bound of look angle. The SAR beam footprint must illuminate the target on Earth, and the covered region must provide valid echoes with a zero-Doppler centroid [5]. Accordingly, the near look angle should be limited within the bound below,

$$\theta_l^{low} < \theta_l^{near} < \theta_l^{up} \qquad (8)$$

$$\theta_l^{up} = \sin^{-1}(R_E R_{SAR}^{-1}) - \lambda k_r l_r^{-1} \qquad (9)$$

$$\theta_l^{low} = \cot^{-1}\left[T_3^{-1} \cdot \sqrt{T_1^2 + T_2^2} \right] \qquad (10)$$

where $T_1 \sim T_3$ are three elements related to the LBSAR motion and Earth rotation; their detailed definitions are given in [5].

From (8)-(10), one yields a bound for determining the beamwidth in the LBSAR, as:

$$\beta < \sin^{-1}\left(R_E R_{SAR}^{-1} \right) - \cot^{-1}\left[T_3^{-1} \cdot \sqrt{T_1^2 + T_2^2} \right] \qquad (11)$$

Taking account of (5) and (11), the aperture length along the range direction must be such that:

$$l_r > l_r^{low} \qquad (12)$$

$$l_r^{low} = \lambda k_r \left[\sin^{-1}(R_E R_{SAR}^{-1}) - \cot^{-1}\left(T_3^{-1} \cdot \sqrt{T_1^2 + T_2^2} \right) \right]^{-1} \qquad (13)$$

We, by far, present the LBSAR swath width based on its observation geometry, followed by deriving relevant bounds in configurations of the LBSAR. In the next section, we shall detail the swath width of LBSAR quantitatively.

3 Quantitative Analysis of Swath Width in the LBSAR

To properly configure the LBSAR, we first examine the bounds that restrict the near-look angle θ_l^{near} and aperture length along the range direction l_r. To be consistent with [9], the carrier frequency was set to 1.2 GHz (L-band), and one LBSAR cycle, corresponding to the epoch from 05:05:29, Mar. 11, 2024, to 16:13:49, Apr. 07, 2024, was selected to investigate both bounds. For simplicity but without loss of generality, we assume that the LBSAR site locates at (0°, 0°) in the MCMF.
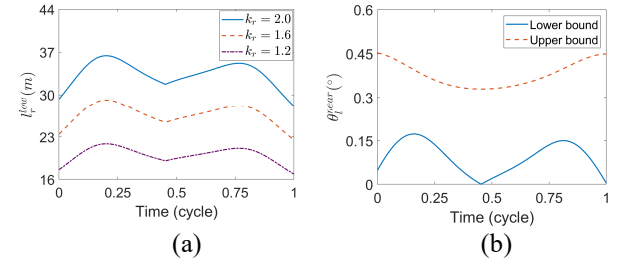

Figure 2. The bounds of l_r and θ_l^{near} within one cycle, (a) the lower bound of l_r under various taper factors; (b) the lower and upper bounds of θ_l^{near}.

Figure 2 (a) plots the bound of aperture length along range direction under various taper factors. We see that the threshold l_r^{low} varies along the orbit of LBSAR, the magnitude of which is positively correlated to the taper factor. Since the threshold l_r^{low} is a lower bound and a higher taper factor requires a larger aperture length, the minimal aperture length along the range direction should be longer than the maximal threshold l_r^{low}. Therefore, in this study, the minimal aperture length l_r was set to 50 m.

Figure 2 (b) presents the low and upper bounds of the near look angle under $l_r = 50\ m$ and $k_r = 2.0$. It can be seen that there exist certain restrictions on the near look angle under specified LBSAR configurations. Further, the lower

and upper bounds of the near look angle vary along the orbit, showing different variation tendencies within the LBSAR cycle. Results also demonstrate that the lower bound of the near look angle is consistently smaller than 0.20°, while the upper bound is persistently larger than 0.30° wherever the LBSAR is located. As such, the near look angle was set to 0.30° in this study.

Now, the quantitative examination of the LBSAR swath width is in order. We first inspect the relationship between the beamwidth and swath width. By so doing, the swath width versus taper factor and aperture length along the range direction at the perigee and apogee are shown in Figure 3 (a) and (b), respectively.
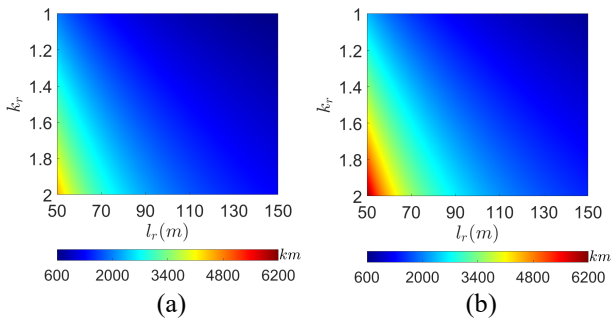
Figure 3. The swath width of the LBSAR versus the taper factor and aperture length along range direction at (a) the perigee, (b) the apogee.

Figure 3 shows that the swath width positively relates to the taper factor while negatively correlating to the aperture length l_r. Besides, at the apogee, the variations of swath width under different beamwidths are more considerable, indicating the LBSAR altitude could affect the influence of beamwidth on swath width. In addition, the distinct beamwidths lead to noticeable variations in the swath width, which can be over thousands of kilometers. Further, the higher taper factor and shorter aperture length make yielding a wider swath width easier. The quantitative assessment shows the swath width can be wider than 4000 km for the L-band LBSAR with a taper factor of 2.0 and an aperture length of 50 m.
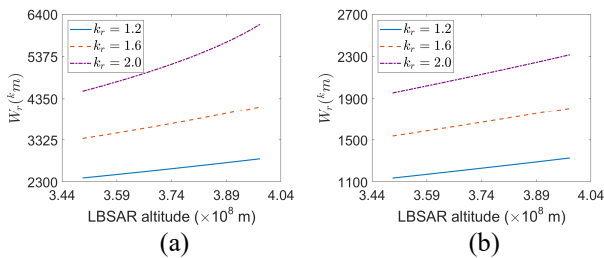
Figure 4. The swath width with various taper factors versus LBSAR altitude under (a) l_r = 50 m, (b) l_r = 100 m.

Next, the influence of LBSAR altitude on the swath width is checked in detail. The swath widths with various taper factors under $l_r = 50\ m$ and $l_r = 100\ m$ are respectively plotted in Figure 4 as a function of the LBSAR altitude. We observe an apparent upward trend in swath width with the increasing LBSAR altitude. Also, the beamwidth could affect the gradient of swath width versus the LBSAR altitude. For a narrower beamwidth, the swath width is quasi-linearly correlated to the LBSAR altitude. In this event, the variation of swath width with respect to the LBSAR altitude is on the order of hundreds of kilometers. By contrast, the LBSAR altitude exerts a high-order effect on the swath width under a wider beamwidth. That is, the maximal fluctuation of swath width within one cycle could be over one thousand kilometers. Taking from the perspective of the results above, the influences of all factors on the LBSAR swath width are all coupled together.

4 The Spatiotemporal Variation of the LBSAR Swath Width in Various Periods

It is known that the orbital elements of the LBSAR are susceptible to perturbation effects [7, 9], which induce variations in the spatiotemporal swath width. To evaluate such effects, we analyze the spatiotemporal variations of the LBSAR swath width along its orbit in different cycles. As the extensive swath width is the major concern of the LBSAR, the aperture length along the range direction and taper factor were set to 50 m and 2.0, respectively.
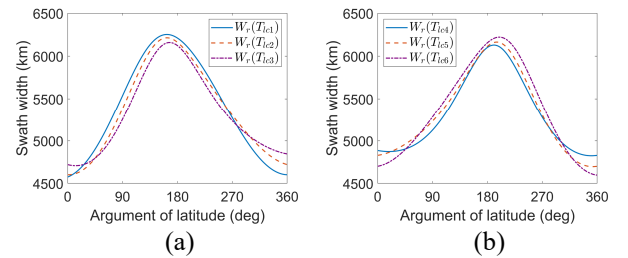

Figure 5. The swath width versus the argument of latitude in three consecutive cycles that correspond to epochs (a) from 05:05:29, Mar. 11, 2024 to 07:59:53, Jun. 1, 2024; (b) from 18:22:18, Jun. 19, 2033 to 19:12:26, Sep. 9, 2033.

The swath width of LBSAR in three consecutive cycles is inspected, shown in Figures 5 (a) and (b). The corresponding swath widths when the orbital inclination approaches its maximum and minimum are plotted as a function of the argument of latitude (AOL). It is observed the swath width varies dramatically about the AOL; the variation magnitude in swath width within one cycle can be over 1000 km. Besides, there are distinct variation tendencies in the swath width in each cycle, and the fluctuation of swath width between each cycle can be up to hundreds of kilometers. Comparisons of Figure 5 (a) to Figure 5 (b) show that after a long period, the fluctuation of the swath width becomes even more prominent. In this regard, the tendencies of the swath width concerning the AOL are irregular, though the swath width is on similar magnitudes. The above phenomena indicate that the orbital perturbations could certainly influence swath width. The accumulation of perturbations effects could further lead to

irregular and aperiodic variations in the spatiotemporal swath width.

The region covered by the LBSAR, which is also dependent on look direction, is checked below. The daily coverages of the LBSAR at maximal and minimal orbital inclinations are simulated and presented in Figure 6 (a) and (b), respectively. In each case, the LBSAR locates at the ascending node when it begins to illuminate Earth.
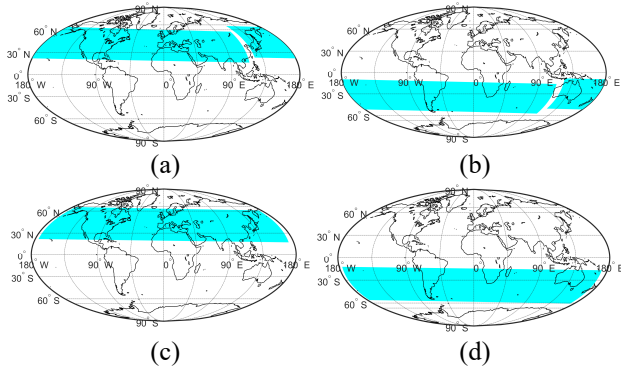
Figure 6. The daily coverage by the LBSAR. The LBSAR looks from (a) left-hand side, (b) right-hand side, with initial illumination time starting at 05:05:29, Mar. 11, 2024; The LBSAR looks from (c) left-hand side, (d) right-hand side, with initial illumination time starting at 18:22:18, Jun. 19, 2033.

The LBSAR shows an outstanding capability of continuously watching Earth with extensive coverage. Besides, the looking side could impact the covered region. Specifically, the left-looking LBSAR mainly views the Earth's northern hemisphere regardless of the orbital inclination. By contrast, the covered region is focused on the southern hemisphere when the LBSAR looks from the right-hand side. In addition, the covered region in the LBSAR shows an irregular variation tendency within one day, indicating that the orbital elements, susceptible to the perturbation effects, could influence the covered region within a specified epoch. The results in Figures 5 and 6 are consistence with the preceding analysis. Further, from the analysis above, we may conclude the spatiotemporal variation of swath width is aperiodic in the LBSAR.

5 Conclusions

This study quantitatively probes into the swath width and its spatiotemporal variation in the LBSAR. The results demonstrate the swath width depends on the LBSAR's altitude and beamwidth in terms of taper factor and aperture length along the range direction. Specifically, the beamwidth could exert positive impacts on swath width. Regarding the LBSAR altitude, it could give rise to a maximal variation of over one thousand kilometers in the swath width within one cycle. As to the covered region on Earth, it is further influenced by the look direction of LBSAR. It is also found that the aperiodic variations appear in the swath width and related coverage even in

consecutive cycles, as the LBSAR altitude is susceptible to orbital perturbations. The long-time accumulations of orbital perturbations lead to more profound and irregular fluctuations in swath width. Notwithstanding, the LBSAR is still expected to yield a swath width over thousands of kilometers and thus maintain continuous coverage of the globe, which is favorable for deepening understanding of our Earth.

Acknowledgements

References

[1] B. Sherwood, "Principles for a practical moon base," *Acta Astronaut.*, **160**, Jul. 2019, pp. 116-124.

[2] A. Moccia and A. Renga, "Synthetic aperture radar for earth observation from a lunar base: Performance and potential applications," *IEEE Trans. Aerosp. Electron. Syst.*, **46**, 3, Jul. 2010, pp. 1034-1051.

[3] G. Fornaro, *et al.*, "Potentials and limitations of moon-borne SAR imaging," *IEEE Trans. Geosci. Remote Sens.,* **48**, 7, Apr. 2010, pp. 3009-3019.

[4] Z. Xu and K.-S. Chen, "Effects of the earth's curvature and lunar revolution on the imaging performance of the moon-based synthetic aperture radar," *IEEE Trans. Geosci. Remote Sens.,* **57**, 8, Mar. 2019, pp. 5868 - 5882.

[5] Z. Xu, K.-S. Chen, and G. Q. Zhou, "Zero-doppler centroid steering for the moon-based synthetic aperture radar: A theoretical analysis," *IEEE Geosci. Remote Sens. Lett.*, **17**, 7, Jul. 2020, pp. 1208 - 1212.

[6] K.-S. Chen, *Principles of Synthetic Aperture Radar: A System Simulation Approach*. Boca Raton, FL, USA: CRC Press, Inc., 2015.

[7] Z. Xu, K.-S. Chen, Z.-L. Li, and G.-Y. Du, "Apsidal precession effects on the lunar-based synthetic aperture radar imaging performance," *IEEE Geosci. Remote Sens. Lett.*, **18**, 6, Jun. 2021, pp. 1079 - 1083.

[8] H. Ye, *et al.*, "Looking vector direction analysis for the moon-based earth observation optical sensor," *IEEE J. Sel. Topics Appl. Earth Observ. Remote Sens.*, **11**, 11, Nov. 2018, pp. 4488-4499.

[9] Z. Xu, K. S. Chen, and G. Liu, "On orbital determination of the lunar-based SAR under apsidal precession," *IEEE Trans. Geosci. Remote Sens.,* **60**, May. 2022, doi: 10.1109/TGRS.2022.3176836.